# A REDUCED ORDER MODEL FOR A STABLE EMBEDDED BOUNDARY PARAMETRIZED CAHN-HILLIARD PHASE-FIELD SYSTEM BASED ON CUT FINITE ELEMENTS

## EFTHYMIOS N. KARATZAS $^{1,2}$ AND GIANLUIGI ROZZA $^1$

ABSTRACT. In the present work, we investigate for the first time with a cut finite element method, a parameterized fourth order nonlinear geometrical PDE, namely the Cahn-Hilliard system. We manage to tackle the instability issues of such methods whenever strong nonlinearities appear and to utilize their flexibility of the fixed background geometry –and mesh– characteristic, through which, one can avoid e.g. in parametrized geometries the remeshing on the full order level, as well as, transformations to reference geometries on the reduced level. As a final goal, we manage to find an efficient global, concerning the geometrical manifold, and independent of geometrical changes, reduced order basis. The POD-Galerkin approach exhibits its strength even with pseudo-random discontinuous initial data verified by numerical experiments.

## 1. Introduction and Motivation

The Cahn–Hilliard model (CH), named after John Cahn and John Hilliard who suggested the system in 1958, describes a prototype of the process of phase separation, by which the two components of a binary fluid or material impulsively separate and form domains, pure in each component. These phase-field systems, are very interesting in the scientific community due to their great conservation properties. They simulate many industrial systems, as the two-phase fluid flows for capturing the interface location between two immiscible fluids, [3, 4, 47], spinodal decomposition in binary alloys—a process in which a mixture of two fluids or materials evolves— [38, 49], and the phase diagram for microphase multiscale separation for diblock copolymer-linear chain molecule consisting of two subchains joined covalently to each other, [21, 48]. Additionally, we mention the image inpainting, i.e., the filling in of damaged or missing regions of an image with the use of information from surrounding areas, [10, 18, 65], micro-structure with elastic inhomogeneity which determines the transformation path and the corresponding microstructure evolution, [74] and references therein, tumor growth simulation in order to provide optimal strategies for treatments, [1, 77], and topology optimization phase-field approach to the problem of minimizing the mean compliance of a multi-material structure, see e.g. [83, 11, 64].

The investigation of the behavior of such systems, started from the pioneer work [16] and the early works of [62, 31, 29]. Thereafter, a lower solution space regularity and a second order splitting method have been investigated in [30], the solution existence and error analysis in [28, 51], for higher order finite element we refer to [34] and for Discontinuous Galerkin in space approach to [76, 60]. Optimal control for non-convective or optimal control for the convective case have been studied in [66, 81, 35, 45, 25, 44], stochastic partial differential equations and stochastic analysis in the very new work of [33], Navier-Stokes/Cahn-Hilliard systems in [46, 43], and Cahn-Hilliard/Allen-Cahn systems in [6, 5, 80, 2].

Throughout this work, an efficient methodology for solving nonlinear systems governed by Cahn–Hilliard equations is studied within cut finite elements and reduced-order modeling. A stable full order scheme for this geometrically parameterized nonlinear fourth-order diffusion system is introduced. In this embedded geometry framework, we propose a model order reduction technique using the advantages of a shape regular background mesh, recently investigated in [52, 55, 54]. The combination of unfitted mesh finite element methods and reduced order modeling allows us to obtain a fast evaluation,

<sup>&</sup>lt;sup>1</sup>SISSA, International School for Advanced Studies, Mathematics Area, mathLab Trieste, Italy.

<sup>&</sup>lt;sup>2</sup>Department of Mathematics, School of Applied Mathematical and Physical Sciences, National Technical University of Athens, Zografou, Greece.

E-mail addresses: karmakis@math.ntua.gr & efthymios.karatzas@sissa.it, grozza@sissa.it.

 $<sup>2010\</sup> Mathematics\ Subject\ Classification.\ 78M34,\ 97N40,\ 35Q35.$ 

Key words and phrases. Cut Finite Element Method, Cahn Hilliard, Reduced Order Model, POD, Stabilization.

by considering the geometrical parametrized system, while we avoid remeshing, as well as the reference domain formulation, often used in boundary fitted finite element formulations.

This contribution is organized as follows: In Section 2 we define the continuous strong formulation of the mathematical problem. The semidiscrete cut elements Nitsche weak formulation and the implicit explicit Euler method (IMEX) fully discrete problem under consideration is introduced, as well as, the incremental scheme used to solve the full order problem during the offline stage. In Section 3, we demonstrate the reduced-order model formulation, based on the Proper Orthogonal Decomposition, and its main aspects. In section 4 the IMEX method and the high fidelity solver efficiency is validated. Subsequently, the proposed ROM technique is tested on a geometrical parametrized problem of a twophase field problem starting from pseudo-random initial data around an embedded circular domain. Convergence results, errors and reduced execution times are introduced and analyzed. Finally in Section 5, conclusions and perspectives for future improvements and developments are demonstrated. To our best knowledge, the results of this work are original and applicable in many cases of nonlinear time-depended partial differential equation problems in terms of the prescribed methodology and in the spirit of the geometrical parametrization.

## 2. The Model problem and the full-order approximation

2.1. Strong formulation of the Cahn-Hilliard problem. We consider the model problem describing a phase flow time evolution. An unknown function u indicates the perturbation of the concentration of one of the phases of fluid components constituting a liquid mixture that contains a binary fluid. Let us consider an open domain  $\Omega$  in  $\mathbb{R}^d$ , with d=2,3 the number of space dimensions with Lipschitz boundary  $\partial\Omega$ . Let a k-dimensional parameter space  $\mathcal{P}$  with a parameter vector  $\mu\in\mathcal{P}\subset\mathbb{R}^k$ . We state below, in a time interval [0,T], the strong form of the evolutionary Cahn-Hilliard phase flow system of equations with open boundary conditions on  $\partial\Omega$ , geometrically parametrized by  $\mu$ . We denote by  $\Omega(\mu)$  and  $\partial\Omega(\mu)$  the parametrized domain and boundary, respectively.

As first suggested by [26], and thereafter extended in [16], if we assume that the mobility is equal to 1 and  $\varepsilon$  is a measure of the size of the interface of two fluids, the mass flux is given by

(1) 
$$\mathbf{J}(\mu) = -\nabla \left( \frac{1}{\varepsilon^2} F(u(\mu)) - \varepsilon^2 \Delta u(\mu) \right),$$

where F denotes the chemical potential difference between the two species. Due to [16], the Ginzburg-Landau energy becomes

(2) 
$$E(u(\mu)) = \int_{\Omega} \left( F(u(\mu)) + \frac{\varepsilon^2}{2} |\nabla u(\mu)|^2 \right) d\mathbf{x}.$$

An equilibrium state of the considered mixture minimizes the above Ginzburg-Landau energy, subject to the mass conservation

(3) 
$$\frac{\partial}{\partial t} \int_{\Omega(\mu)} u(\mu) d\mathbf{x} = 0.$$

Hence, the parametrized Cahn–Hilliard system can be described as:

(4) 
$$\frac{\partial u(\mu)}{\partial t} = -\varepsilon^2 \Delta^2 u(\mu) + \frac{1}{\varepsilon^2} \Delta F'(u(\mu)), \quad \text{in } \Omega(\mu) \times [0, T],$$
(5) 
$$\partial_n u(\mu) = \partial_n (-\varepsilon^2 \Delta u(\mu) + \frac{1}{\epsilon^2} F'(u(\mu))) = g_N(\mu), \quad \text{on } \partial \Omega(\mu) \times [0, T],$$
(6) 
$$u(\cdot, 0) = u_0(\cdot), \quad \text{in } \Omega(\mu),$$

(5) 
$$\partial_n u(\mu) = \partial_n (-\varepsilon^2 \Delta u(\mu) + \frac{1}{\varepsilon^2} F'(u(\mu))) = g_N(\mu), \quad \text{on } \partial \Omega(\mu) \times [0, T],$$

(6) 
$$u(\cdot,0) = u_0(\cdot), \quad \text{in } \Omega(\mu),$$

where n is the unit outer normal vector of  $\partial\Omega$ , and F is a double-well usually taken as a polynomial function of u of fourth power:

(7) 
$$F(u(\mu)) = \gamma_2 \frac{u^4(\mu)}{4} + \gamma_1 \frac{u^3(\mu)}{3} + \gamma_0 \frac{u^2(\mu)}{2} \text{ with } \gamma_2 > 0.$$

For more details, the interested reader is referred to [31] as well as for Dirichlet boundary conditions in [61]. We remark that the equation (4) represents the equation of conservation of mass, with mass flux as described in (1).

# 2.2. Full-order parametrized Nitsche cut elements weak variational formulation.

2.2.1. A proper continuous weak formulation. The Cahn-Hilliard equation as it is expressed in Equations (4)-(6) is a fourth-order diffusion equation, involving first-order time derivatives, second and fourth-order spatial derivatives. Casting it in a weak form results in second-order spatial derivatives avoiding the fourth-order ones. Nevertheless, the problem still can not be solved using the standard Lagrange finite element basis. The setback also is that if someone employs the Nitsche weak boundary enforcement, several integrals in the cut geometry should be calculated including various order derivatives and normal derivatives, [76, 32, 82, 41], which in our case of unfitted mesh are avoided due to time expensive integration. Moreover, a special stabilization term for the nonlinearity would be needed, [24, 13].

To overcome all these difficulties arising from this fourth-order nonlinear system, firstly we employ a splitting method deriving a strong formulation system that requires  $H^2$  space regularity. Afterward, we multiply with a test function and we integrate by parts over  $\Omega$  in order to drive the system to a weak form that requires only  $H^1$  space regularity. In particular the pair solution  $(u(\mu), w(\mu))$ solves the following problem: find  $u(\mu) \in L^2[0,T;H^1(\Omega(\mu))] \cap H^1[0,T;(H^1(\Omega(\mu)))']$  and  $w(\mu) \in L^2[0,T;H^1(\Omega(\mu))]$  $L^2[0,T;H^1(\Omega(\mu))]$  for all weight functions  $v(\mu)\in H^1(\Omega(\mu))$  such that

(8) 
$$(\frac{\partial u(\mu)}{\partial t}, v(\mu)) + (\nabla w(\mu), \nabla v(\mu)) = (g_N(\mu), v(\mu))_{\partial \Omega(\mu)},$$
(9) 
$$-(w(\mu), v(\mu)) + \varepsilon^2 (\nabla u(\mu), \nabla v(\mu)) + \varepsilon^{-2} (F'(u(\mu)), v(\mu)) = (g_N(\mu), v(\mu))_{\partial \Omega(\mu)},$$

$$(9) \qquad -(w(\mu), v(\mu)) + \varepsilon^2(\nabla u(\mu), \nabla v(\mu)) + \varepsilon^{-2}(F'(u(\mu)), v(\mu)) = (g_N(\mu), v(\mu))_{\partial\Omega(\mu)}$$

$$(10) u(\cdot,0;\mu) = u_0(\cdot;\mu),$$

where  $w(\mu)$  is depended on the geometry parameter  $\mu$  and usually it is identified as a chemical potential,  $\forall v \in H^1(\Omega(\mu))$  and  $u_0 \in L^2(\Omega(\mu))$ . In the following, we are focused on the concentration component  $u(\mu)$ , and we handle  $w(\mu)$  as auxiliary function. Similarly, Dirichlet boundaries will be examined following [61].

Remark 2.1. We point out that we are taking into account nonsmooth initial data  $L^2(\Omega(\mu))$  while the aforementioned regularity  $H^1[0,T;(H^1(\Omega(\mu)))']$  of  $u(\mu)$  is needed for the  $\partial u(\mu)/\partial t$  term<sup>1</sup>, see [22, 23].

2.2.2. Discretization, unfitted mesh and stability issues. The system (8)-(9) in a discrete unfitted mesh formulation needs extra attention. Even if we use classical finite element methods and we apply the boundary conditions in a strong way, stability issues appear, and to achieve a stable solution a quite small time-stepping size seems necessary. We highlight that the evolution of the physics of the problem during the first time steps is very fast, although, as time passes it slows down and finally it equilibrates, see also e.g. [78, 12], and references therein. An adaptive time-stepping approach would appear beneficial, although we will investigate it in a future work, as well as, the way it affects the accuracy and efficiency of the reduced model detailed in Sections 3 and 4. Considering the Nitsche terms one may apply the simple formulation needed for linear systems. Under these considerations, we used cut finite element methods to solve the system applying a jump stabilization procedure in the boundary elements interface area. In the next paragraph, we derive the semi-discrete formulation of the system, while in paragraph 2.2.4 the fully discrete system is exploited.

2.2.3. Semidiscrete variational formulation. We denote by  $\mathcal{T}$  the background domain, and by  $\mathcal{T}_h$  its corresponding mesh, see e.g. Figure 1. Considering the standard notation  $(\cdot, \cdot)$ ,  $\langle \cdot, \cdot \rangle_{\partial\Omega}$  for the  $L^2(\Omega)$ , and  $L^2(\partial\Omega)$  inner products onto the truth geometry  $\Omega$ , and  $\partial\Omega$ , respectively. For every element  $K \in \mathcal{T}_h$ , we associate a parameter  $h_K$ , denoting the diameter of the set K. The size of the mesh is denoted by  $h = \max_{K \in \mathcal{T}_h} h_K$ .

The continuous boundary value problem is next formulated on a domain  $\tilde{\Omega}(\mu)$  that contains  $\Omega(\mu) \subset$  $\tilde{\Omega}(\mu)$ , while its mesh  $\tilde{\Omega}_{\mathcal{T}}(\mu) := \mathcal{T}_h \cap \tilde{\Omega}(\mu)$  is not fitted to the domain boundary and  $\tilde{\Omega}_{\mathcal{T}}(\mu) \subset \mathcal{T}$  for all  $\mu \in \mathcal{K}$ . Let also  $\Omega_{\mathcal{T}}(\mu) := \mathcal{T}_h \cap \Omega(\mu)$  and  $G_h(\mu) := \{K \in \mathcal{T}_h(\mu) : K \cap \partial \Omega(\mu) \neq \emptyset\}$  be the set of elements that are intersected by the interface. We remark that  $G_h(\mu)$  and  $\Omega_T(\mu)$  depend on  $\mu$  through  $\tilde{\Omega}(\mu)$  (or its boundary), while the background domain  $\mathcal{T}$  and its mesh  $\mathcal{T}_h$  do not depend on  $\mu$ .

Furthermore, the set of element faces  $\mathcal{F}_G(\mu)$  associated with  $G_h(\mu)$ , is defined as follows: for each face  $F \in \mathcal{F}_G(\mu)$ , there exist two simplices  $K \neq K'$ , such that  $F = K \cap K'$ , and at least one of the two is a member of  $G_h(\mu)$ . Note that the boundary faces of  $\Omega_T(\mu)$  are excluded from  $\mathcal{F}_G(\mu)$ . On a face  $F \in \mathcal{F}_G(\mu), F = K \cap K'$ , the jump of v is defined by  $[v] = v|_K - v|_{K'}$  and the jump of the gradient  $[\![\mathbf{n}_F \cdot \nabla v]\!] = \mathbf{n}_F \cdot \nabla v|_K - \mathbf{n}_F \cdot \nabla v|_{K'}$ , where  $\mathbf{n}_F$  denotes the outward pointing unit normal vector to F.

<sup>&</sup>lt;sup>1</sup>namely,  $\partial u(\mu)/\partial t \in L^2[0,T;(H^1(\Omega(\mu)))'].$ 

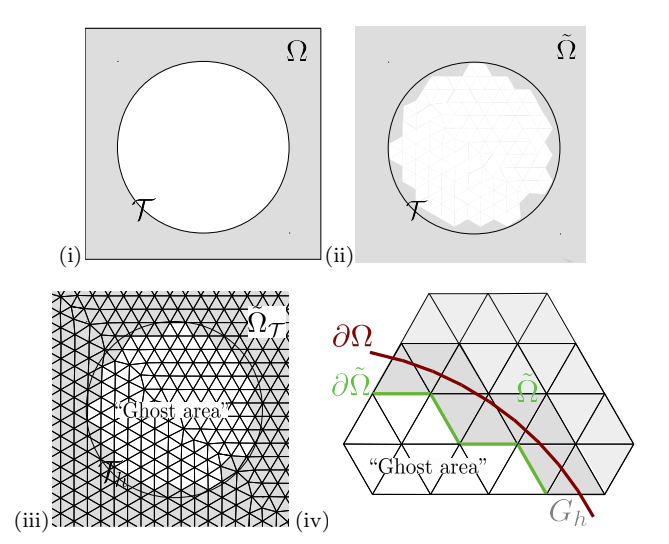


FIGURE 1. (i) The geometry of an embedded disk, (ii) the cut finite element method geometry, (iii) zoom on the background mesh together with the surrogate cut discretized geometry, and (iv) extended mesh and elements intersected by the true boundary.

Let the space of continuous piecewise-linear functions  $\mathcal{V}_h(\Omega(\mu))$ 

(11) 
$$\mathcal{V}_h(\Omega(\mu)) = \left\{ v \in C^0(\overline{\Omega}_{\mathcal{T}}(\mu)) : v|_K \in P^1(K), \forall K \in \mathcal{T}_h(\mu) \right\}.$$

For the sake of simplicity, in the next set of equations, we will omit the parameter dependency notation with respect to  $\mu$  and the CutFEM discretization is as follows. We seek  $u_h, w_h \in \mathcal{V}_h(\tilde{\Omega}(\mu))$  such that, for all the test functions  $v_h, q_h \in \mathcal{V}_h(\tilde{\Omega}(\mu))$ ,

$$(u_{ht}, v_h) + (\nabla w_h, \nabla v_h) + \varepsilon^2 (\nabla u_h, \nabla q_h) - (w_h, q_h) + \frac{1}{\varepsilon^2} (\gamma_2 u_h^3 + \gamma_1 u_h^2 + \gamma_0 u_h, q_h)$$

$$+ \langle \alpha_N h \mathbf{n}_{\Omega} \cdot \nabla u_h, \mathbf{n}_{\Gamma} \cdot \nabla v_h \rangle_{\partial \Omega} + \sum_{F \in \mathcal{F}_G} (\alpha_1 h^{-2} \llbracket u_h \rrbracket, \llbracket v_h \rrbracket)_F$$

$$= \langle g_N, v_h + q_h + \alpha_N h \mathbf{n}_{\Gamma} \cdot \nabla v_h \rangle_{\partial \Omega},$$

$$(12)$$

where  $\alpha_N$ , and  $\alpha_1$  are positive penalty parameters related to Nitsche weak imposition of boundary conditions and the boundary interface stabilization term respectively, see for instance [14].

Remark 2.2. For the sake of completeness, it would be convenient to emphasize that both the aforementioned kind of "jumps", can be used to apply different type of ghost penalty stabilizations, namely  $\sum_{F \in \mathcal{F}_G} (\alpha_1 h \llbracket \mathbf{n}_F \cdot \nabla u_h \rrbracket)_F$  and  $\sum_{F \in \mathcal{F}_G} (\alpha_1 h^{-2} \llbracket u_h \rrbracket)_F$ . Although, we prefer to employ the "projection based"-jump and not the "derivative"-jump one. All experiments consider first order polynomials. Finally, we highlight that the preferred ghost penalty is less computational expensive since it does not involve any kind of derivatives. Concerning literature, most theoretical estimates are related to the "derivative-jump", nevertheless, they can easily be extended to the "projection based"-jump ghost penalty since the jump can be bounded from above with the derivative jump, for more details we refer to [13, 15, 73, 59].

2.2.4. IMEX type time discretization. The goal here is to find concentration  $u_h = u_h(x,t)$  satisfying the equations (12) for all time instances t in a time interval  $[0,T] \subset \mathbb{R}$  and space positions  $x \in \Omega \subset \mathbb{R}^d$ . We fully discretize the system by an IMEX approach, see e.g. [67] and references therein, as well as [57] for similar types of nonlinearities. Approximations will be constructed on a time partition  $0 = t^0 < t^1 < \ldots < t^N = T$  on which, each interval  $I_n := (t^n, t^{n+1}]$  is of length  $\tau_n = t^{n+1} - t^n$ ,  $n = 1, \ldots, N-1$ , starting from initial condition  $u^0$ . Therefore, we apply a splitting method onto time integration level –often called operator splitting method– which means that the differential operator is rewritten as the sum of two complementary operators. The latter extensively attracted attention IMEX method technique treats on the nonlinear term explicitly, allowing to act as a forcing term in the w-equation (8). In this way, we avoid stability issues caused by the nonlinearity. All the other

terms have been handled implicitly for better accuracy. Hence, the IMEX method results in the set of fully-discrete Cahn-Hilliard equations:

Find 
$$(u_h^{n+1}, w_h^{n+1}) \in \mathcal{V}_h \times \mathcal{V}_h$$
, s.t. for all  $(v_h^n, q_h^n) \in \mathcal{V}_h \times \mathcal{V}_h$   

$$A(u_h^{n+1}) + \tau_n \cdot L(u_h^{n+1}, w_h^{n+1}) = A(u_h^n) - \tau_n \cdot N(u_h^n) + B(g_N) \cdot \tau_n,$$

where

$$\begin{array}{lcl} A(u_{h}^{n+1}) & = & (u_{h}^{n+1}, v_{h}^{n+1}) = \mathbf{A}u_{h}^{n+1}, \\ L(u_{h}^{n+1}, w_{h}^{n+1}) & = & (\nabla w_{h}^{n+1}, \nabla v_{h}^{n+1}) + \varepsilon^{2}(\nabla u_{h}^{n+1}, \nabla q_{h}^{n+1}) - (w_{h}^{n+1}, q_{h}^{n+1}) \\ & & + \langle \alpha_{N}h\mathbf{n}_{\Omega}\cdot\nabla u_{h}^{n+1}, \mathbf{n}_{\Gamma}\cdot\nabla v_{h}^{n+1}\rangle_{\partial\Omega} + \sum_{F\in\mathcal{F}_{G}}\left(\alpha_{1}h^{-2}\llbracket u_{h}\rrbracket, \llbracket v_{h}\rrbracket\right)_{F} \\ & = & \mathbf{L}_{1}u_{h}^{n+1} + \mathbf{L}_{2}w_{h}^{n+1} + \mathbf{C}_{\mathcal{F}_{\mathbf{G}}}u_{h}^{n+1}, \\ B(g_{N}) & = & \langle g_{N}, v_{h}^{n} + q_{h}^{n} + \alpha_{N}h\mathbf{n}_{\Gamma}\cdot\nabla v_{h}^{n}\rangle_{\partial\Omega} = \mathbf{B}_{v} + \mathbf{B}_{q}, \\ N(u_{h}^{n}) & = & \frac{1}{\varepsilon^{2}}(\gamma_{2}u_{h}^{n3} + \gamma_{1}u_{h}^{n2} + \gamma_{0}u_{h}^{n}, v_{h}^{n}) = \mathbf{N}(u_{h}^{n})u_{h}^{n}. \end{array}$$

Next, we derive the related to that system matrix form. We define the parameter-depended Cahn-Hilliard operator

$$G(U_h^n(\mu)) := G\left(\begin{bmatrix} u_h^n(\mu) \\ w_h^n(\mu) \end{bmatrix}\right) = \begin{bmatrix} \mathbf{L_1} + \mathbf{N}(u_h^n(\mu)) & \mathbf{L_2} \\ \mathbf{C}_{\mathcal{F}_{\mathbf{G}}} & 0 \end{bmatrix} \begin{bmatrix} u_h^n(\mu) \\ w_h^n(\mu) \end{bmatrix},$$

and the right hand side consists of the forcing boundary data related to stabilization and Nitsche weak enforcement boundary terms  $F_N(\mu) := \begin{bmatrix} \mathbf{B}_v(\mu) \\ \mathbf{B}_q(\mu) \end{bmatrix}$ . These definitions result in the following residual

$$R(U_h^n(\mu)) = G(U_h^n(\mu)) - F_N(\mu),$$

which yield the following algebraic system of equations for the increment  $\delta U_h^{n+1}(\mu) = \begin{bmatrix} \delta u_h^n(\mu) \\ \delta w_h^n(\mu) \end{bmatrix} = U_h^{n+1}(\mu) - U_h^n(\mu)$ :

(13) 
$$\begin{bmatrix} \mathbf{A} + \tau_n \mathbf{L_1} & \tau_n \mathbf{L_2} \\ \tau_n \mathbf{C}_{\mathcal{F}_{\mathbf{G}}} & 0 \end{bmatrix} \delta U_h^{n+1}(\mu) = -\tau_n R(U_h^n(\mu)),$$

noting that in the above formulation the nonlinear term is treated only explicitly and the remaining part implicitly.

Remark 2.3. IMEX method approach is beneficial since we avoid the extra computation of iterative approaches, e.g. Newton-Raphson method, and simultaneously we avoid the small-time stepping of an explicit time integration method, needed for a stable solution in order to minimize the dispersion error associated with these schemes. In the above system of equations, it is important to underline that the discretized differential operators A,  $L_1$ ,  $L_2$  and  $C_{\mathcal{F}_{\mathbf{G}}}$  are parameter-dependent, a feature of great importance as we will see in Section 3 and the ROM basis construction. Also, a pre-assembling technique for the involved matrices will be employed in Section 4, by minimizing the time-consuming integration of several involved inner products.

## 3. Reduced order model with a POD-Galerkin method

In this paragraph, a POD-Galerkin approach is briefly recalled as in [42, 68]. We emulate the high fidelity model system with a reproduced one, which allows predictive errors, within the aim of a reduced computational cost and solution time in a way adjusted to embedded-immersed boundary finite element methods. This reduced-order system has been approved advantageous when geometrically deformed systems appear and in comparison with traditional finite element methods and/or reduced-order modeling, see for instance [7, 52, 54, 55]. In particular, we employ a projection-based reduced order model which consists of the projection of the governing equations onto the reduced basis space constructed on a fixed background mesh.

Following the literature, one could see reduced basis (RB) methods applied to linear elliptic equations in [70], to linear parabolic equations in [37] and to non-linear problems in [75, 36]. Although the number of works on reduced-order models with classical FEM are now significant big including Cahn-Hilliard systems, see e.g. [35, 42, 68, 70, 37, 75, 36] and references therein, to the best of the authors' knowledge, only very few research works [7, 52, 54, 55, 56] can be found concerning embedded boundary methods on linear systems and ROMs and much fewer for nonlinear, [56, 53]. So, for the first time we investigate

6

and focus onto how we can achieve for a fourth order evolutionary Cahn–Hilliard PDE system, in a Full Order Method (FOM) and in a Reduced Order Model (ROM) framework, a stable solution within an embedded finite element method namely in a cut finite elements setting. The new techniques of [52, 54, 55], based on a proper orthogonal decomposition (POD) strategy will be employed. The key feature of our approach is that we avoid the remeshing effort or/and the need of a map of all the deformed geometries to reference geometries often used in fitted mesh finite element methods, see e.g. [42, 72, 69, 8, 71, 70, 9].

Regarding the reduced-order modeling, we investigate how ROMs can be applied to time depended cut finite element methods and generally, to embedded boundary methods simulations considering time depended nonlinear systems and Cahn–Hilliard systems. The main interest is to generate ROMs on parametrized geometries. The cut elements unfitted mesh finite element method with levelset geometry description is used to apply parametrization and the reduced order techniques (offline-online). An important aspect is also to test the efficiency of a geometrically parametrized reduced-order nonlinear model without the usage of the transformation to reference domains, which is an important advantage of embedded methods relying on fixed background meshes.

Before going into thorough, we specify some basics for reduced basis modeling. We always start by the generation of a set of full order solutions of the parametrized problem under a parameter values random choice. The final objective of RB methods is to emulate any member of this solution set with a low number of basis functions and this is based on a two-stage procedure, the offline and the online stage, [63, 72, 39].

Offline stage. In order to derive reduced-order solutions emulating the full order system, a low dimensional reduced basis is constructed based on a specific number of full order solves. This reduced basis will be able to approximate any member of the solution set to a predictive error accuracy. Hence, it is possible to project the FOM differential operators, describing the governing equations, onto the reduced basis space, applying a Galerkin projection technique and to create a reduced system of equations. The offline stage is computationally very expensive, nevertheless, it is executed only once.

Online stage. Thereafter, during this stage, one can, even with very few computational resources, calculate a reproduced reduced system of equations involving any new value of the input parameters. For more details and applications, we refer to [9, 19] and the references therein.

3.1. **POD.** The full-order model, as illustrated in paragraph 2.2.4, is solved for each  $\mu^k \in \mathcal{K} = \{\mu^1, \dots, \mu^{N_k}\} \subset \mathcal{P}$  where  $\mathcal{K}$  is a finite-dimensional training set of parameters chosen inside the parameter space  $\mathcal{P}$ . The considered problem can be simultaneously parameter and time-dependent. In order to collect snapshots for the generation of the reduced basis spaces, one needs to consider both the time and parameter dependency. For this reason, discrete-time instants  $t^k \in \{t^1, \dots, t^{N_t}\} \subset [0, T]$  belong in a finite-dimensional training set, which is a subset of the simulation time interval and are considered as parameters. The total number of the full order snapshots is then equal to  $N_s = N_k \cdot N_t$ . The snapshots matrices  $\mathcal{S}_{\boldsymbol{u}}$  and  $\mathcal{S}_{\boldsymbol{w}}$ , are then given by  $N_s$  full-order snapshots:

(14) 
$$\mathbf{S}_{u} = [u(\mu^{1}, t^{1}), \dots, u(\mu^{N_{r}}, t^{N_{t}})] \in \mathbb{R}^{N_{u}^{h} \times N_{s}},$$

(15) 
$$\mathbf{S}_{w} = [w(\mu^{1}, t^{1}), \dots, w(\mu^{N_{r}}, t^{N_{t}})] \in \mathbb{R}^{N_{w}^{h} \times N_{s}},$$

where  $N_u^h$  and  $N_w^h$  are the number of degrees of freedom for the discrete full-order solution for the concentration u and the auxiliary variable w, respectively. The reduced-order problem can be efficiently solved for both sets of parameters and time instants. In order to generate the reduced basis spaces, for the projection of the governing equations, one can find in literature several techniques such as the Proper Orthogonal Decomposition (POD), the Proper Generalized Decomposition (PGD) and the Reduced Basis (RB) with a greedy sampling strategy. For more details about the different strategies the reader may see [42, 70, 19, 50, 63, 20, 27]. In this work, the POD strategy is applied onto the full snapshots matrices. The aforementioned procedure includes both time and parameter dependency. In the case of parametric and time-dependent problems also other approaches are available such as the POD-Greedy approach [39] or the nested POD approach, where the POD is applied first in the time domain and then on the parameter space. Given a general scalar u(t) in  $\mathbb{R}^d$ , with a certain number of realizations  $u_1, \ldots, u_{N_s}$ , the POD problem consists in finding, for each value of the dimension of POD space  $N_{POD} = 1, \ldots, N_s$ , the scalar coefficients  $a_1^1, \ldots, a_{1}^{N_s}, \ldots, a_{N_s}^{N_s}$  and functions  $\varphi_1, \ldots, \varphi_{N_s}$ 

minimizing the quantity:

(16) 
$$E_{N_{POD}} = \sum_{i=1}^{N_s} ||u_i - \sum_{k=1}^{N_{POD}} a_i^k \varphi_k|| \quad \forall N_{POD} = 1, \dots, N,$$

(17) with 
$$\langle \varphi_i, \varphi_j \rangle_{L_2(\Omega)} = \delta_{ij} \quad \forall i, j = 1, \dots, N_s$$
.

The detailed results for the auxiliary variable w are omitted for shortness of space. It can be shown, [58], that the minimization problem of Equation (16) is equivalent of solving the following eigenvalue problem:

$$C^{u}Q^{u} = Q^{u}\lambda^{u},$$

(19) 
$$C_{ij}^{u} = \langle u_i, u_j \rangle_{L_2(\Omega)} \quad \text{for } i, j = 1, \dots, N_s,$$

where  $\mathcal{C}^u$  is the correlation matrix obtained starting from the snapshots  $\mathcal{S}_u$ ,  $Q^u$  is a square matrix of eigenvectors and  $\lambda^u$  is a vector of eigenvalues. The basis functions can then be obtained with:

(20) 
$$\varphi_i = \frac{1}{N_s \lambda_i^u} \sum_{i=1}^{N_s} u_j Q_{ij}^u.$$

The POD spaces are constructed using the aforementioned methodology resulting in the spaces:

(21) 
$$\mathbf{\mathcal{B}}_{u} = \operatorname{span}\{\varphi_{1}, \dots, \varphi_{N^{r}}\} \in \mathbb{R}^{N_{u}^{h} \times N_{u}^{r}},$$

and similarly for the auxiliary variable:

(22) 
$$\mathbf{\mathcal{B}}_{w} = \operatorname{span}\{\chi_{1}, \dots, \chi_{N_{w}^{r}}\} \in \mathbb{R}^{N_{p}^{h} \times N_{w}^{r}},$$

where  $N_u^r$ ,  $N_w^r < N_s$  are chosen according to the eigenvalue decay of the vectors of eigenvalues  $\lambda^u$  and

Once the POD functional spaces are set, the reduced quantities fields can be approximated with:

(23) 
$$u^r \approx \sum_{i=1}^{N_u^r} a_i(t,\mu) \varphi_i(\mathbf{x}), \quad w^r \approx \sum_{i=1}^{N_w^r} b_i(t,\mu) \chi_i(\mathbf{x}),$$

where the coefficients  $a_i$  and  $b_i$  depend only on the time and parameter spaces and the basis functions

$$\varphi_i$$
 and  $\chi_i$  depend only on the physical space and not on the parametrized geometry.

By denoting  $\mathcal{B} = \begin{bmatrix} \mathcal{B}_u & \mathbf{0} \\ \mathbf{0} & \mathcal{B}_w \end{bmatrix}$  and  $\mathcal{B}^T = \begin{bmatrix} \mathcal{B}_u^T & \mathbf{0} \\ \mathbf{0} & \mathcal{B}_w^T \end{bmatrix}$ , the unknown vectors of coefficients  $V = \begin{bmatrix} \mathbf{a} \\ \mathbf{b} \end{bmatrix}$ 

then can be obtained through a Galerkin projection of the full-order system of equations onto the POD reduced basis spaces with the resolution of a consequent reduced iterative algebraic system of equations for the increment  $\delta V_h^{n+1}(\mu) = V_h^{n+1}(\mu) - V_h^n(\mu)$ ,

(24) 
$$\mathcal{B}^{T} \begin{bmatrix} \mathbf{A} + \tau_{n} \mathbf{L}_{1} & \tau_{n} \mathbf{L}_{2} \\ \tau_{n} \mathbf{C}_{\mathcal{F}_{\mathbf{G}}} & 0 \end{bmatrix} \mathcal{B} \delta V_{h}^{n+1}(\mu) = -\tau_{n} \mathcal{B}^{T} R(\mathcal{B} V_{h}^{n}(\mu)),$$

which leads to the following algebraic reduced system:

(25) 
$$\begin{bmatrix} \mathbf{A} + \tau_n \mathbf{L_1} & \tau_n \mathbf{L_2} \\ \tau_n \mathbf{C}_{\mathcal{F}_{\mathbf{G}}} & 0 \end{bmatrix}^r \delta V_{h,r}^{n+1}(\mu) = -\tau_n R^r(V_{h,r}^n(\mu)).$$

Remark 3.1. The initial conditions for the ROM system of equation (25) are obtained performing a Galerkin projection of the initial full-order condition  $u(\cdot,0;\mu)$ ,  $w(\cdot,0;\mu)$  onto the POD basis spaces. For an efficient ROM basis construction, we follow some ideas of the authors as demonstrated in [52]. In particular, concerning the full order method snapshots extension, and the extension of the solution to the surrogate domain into the ghost area, we use the solution values as they have been computed using the cut finite element method smooth mapping from the true to the unfitted mesh domain. This approach allows a smooth extension of the boundary solution to the neighboring ghost elements with values which are decreasing smoothly to zero, see for instance the zoomed image in Figure 3.

This approach provides a regular solution in the background domain and permits, therefore, the construction of a "functional" reduced basis.



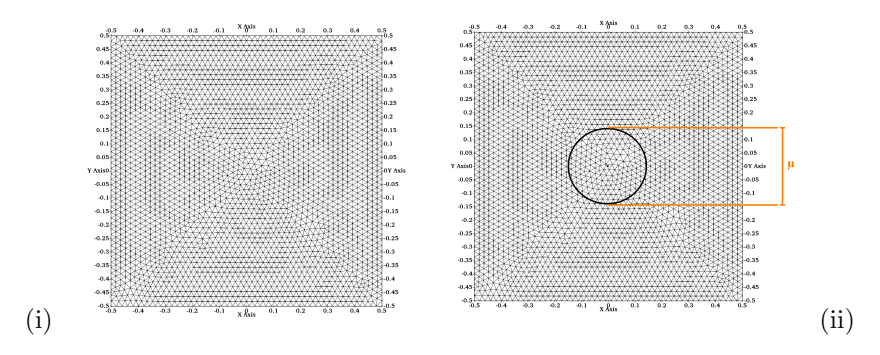


FIGURE 2. The background mesh (i), and a sketch of the embedded domain and the parameters considered in the numerical examples (ii).

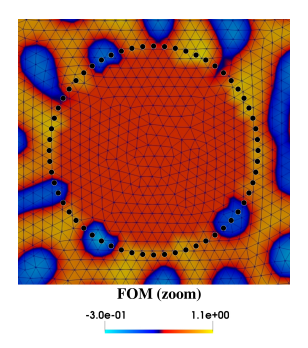


FIGURE 3. A zoom onto the embedded circular domain of the numerical example shows the smoothing natural smooth extension procedure employed by the cut finite element method inside the ghost area.

#### 4. Numerical experiments

In the present section, we test the presented methodology considering numerical experiments for the evolutionary Cahn-Hilliard system while natural homogeneous Neumann boundary conditions, and/or zero Dirichlet ones are present. We start by testing the robustness of the full order model (FOM) for two classical benchmark test cases and we continue with a numerical example in which geometrical parametrization for the embedded domain is considered. The background domain in all experiments is the rectangle  $[-0.5, 0.5] \times [-0.5, 0.5]$ , and the double well fourth power polynomial parameters  $\gamma_0$ ,  $\gamma_1$  and  $\gamma_2$  according to formula (7), are taken as  $\gamma_0 = 2$ ,  $\gamma_1 = 9$  and  $\gamma_2 = 4$ , with the two fluids interface size  $\varepsilon = 10^{-2}$ . The results for all test problems have been obtained with mesh size h = 1/48 unless otherwise stated, Nitsche parameter  $a_N = 10$  and jump stabilization parameter  $a_1 = 0.1^3$ .

4.1. Robustness of the FOM solver. In this first numerical example, we test the validity of the full order solver and the IMEX method. Two benchmark tests are examined, [43, 34, 79], a cross-shaped and an ellipse-shaped phase-field interface applying time step  $\tau_n = \mathcal{O}(10^{-8})$ , for 10000 and 7000 time steps respectively and without any embedded geometry, see Figure 2 (i). For the first experiment, we consider the initial state

e initial state 
$$u_0(x,y) = \begin{cases} 0.6, & \text{if } 5 |(y-0.5) - \frac{2}{5}(x-0.5)| + |\frac{2}{5}(x-0.5) - (y-0.5)| \leq 1, \\ 0.6, & \text{if } 5 |(x-0.5) - \frac{2}{5}(y-0.5)| + |\frac{2}{5}(y-0.5) - (x-0.5)| \leq 1, \\ 0, & \text{otherwise,} \end{cases}$$

and for the second ellipse-shaped interface the initial data

$$u_0(x,y) = -\tanh(((x-0.5)/0.35^2)^2 + ((y-0.5)/0.1^2)^2 - 1).$$

In both cases, with elliptic, and with the additional difficulty of presenting sharp corners in a cross-shaped interface case, we observe evolution toward to a circular interface, see Figures 4, 5, that validates the efficiency of the FOM methodology. For these benchmark tests, we also refer to the work [17].

Remark 4.1. Moreover, we emphasize that the cut elements FEM stabilization robustness is additionally verified using the conservation of mass test, as it is illustrated in the next paragraph numerical experiment. In particular, in Figure 12, we can easily notice that the FOM solution and in particular

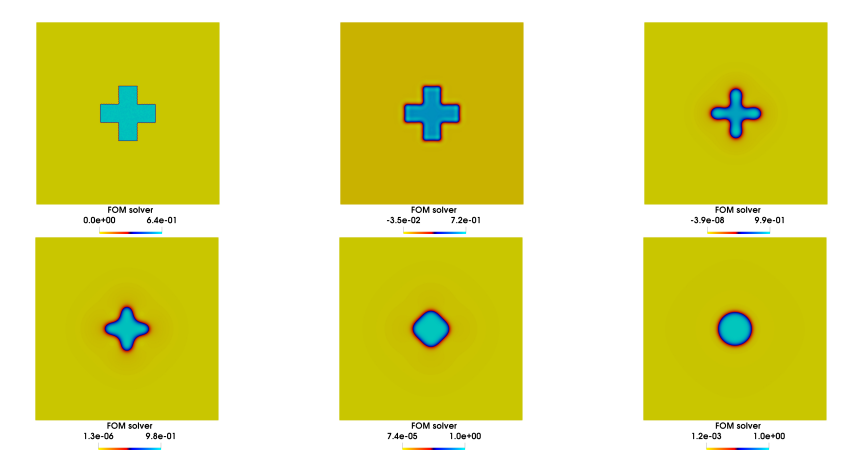


FIGURE 4. Testing the IMEX method: Cross type initial data and the phase field results for times  $t = [0, 10, 1300, 3000, 5000, 10000]\tau_n$  which visualizes that it evolves efficiently to a circular interface.

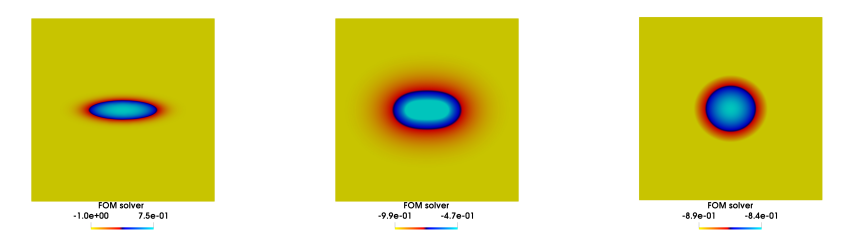


FIGURE 5. Testing the IMEX method: Ellipse type initial data and the phase-field results for times  $t = [0,600,7000]\tau_n$  which visualizes that it evolves efficiently to a circular interface.

the mass preserves very well, as time passes fulfilling the conservation of mass property (see Equation 3).

4.2. Geometrical parametrization. The numerical examples consider a geometrical parametrization on the embedded domain. The embedded domain is in fact parametrized through  $\mu$  according to the expression:

$$x^2+y^2 \leq \mu^2/4,$$

where the parameter  $\mu$  describes the diameter size of the circular embedded domain located on the center (0,0) of the background domain, see e.g. Figure 2 (ii). The experiments focus on the initial evolution period when the phase-field changes fast, namely in the time interval  $0-100~\tau_n$  for time step size  $\tau_n=\mathcal{O}(10^{-6})$ . We tested pseudo-random initial concentration u data and zero initial data for the auxiliary variable w. For all parameters, we experimented the same pseudo-random initial state applied on the whole background mesh and afterward restricted onto the active parametrized geometry. In the first experiment the boundaries are free (open boundary condition) everywhere, while in the second one we consider Dirichlet only for the embedded geometry, [61]. Though, only the cylinder is treated as embedded. Linear  $\mathbb{P}1 \times \mathbb{P}1$  polynomials have been employed for the discretization. During the initial period of the evolution,  $[0,T]=[0,100\tau_n]$ , someone can notice fast phase-field changes starting from pseudo-random initial data, both challenging for the ROM construction. Nevertheless, as time passes these changes are weakened, see e.g. Figure 6 for a visualization of the evolution of an open and a Dirichlet type embedded boundary.

For the reduced basis solution, the ROM has been trained onto 900 parameter samples and tested onto 30 samples in a parameter range  $\mu_{\text{test}} \in [0.36, 0.48]$  chosen randomly inside the parameter space. From these snapshots selection, a ROM basis has been derived with a POD procedure. The visualization of the first six basis components can be seen in Figure 7. To test the accuracy of the ROM we compared its results on 30 additional samples which were not used to create the ROM and were selected randomly within the aforementioned range.

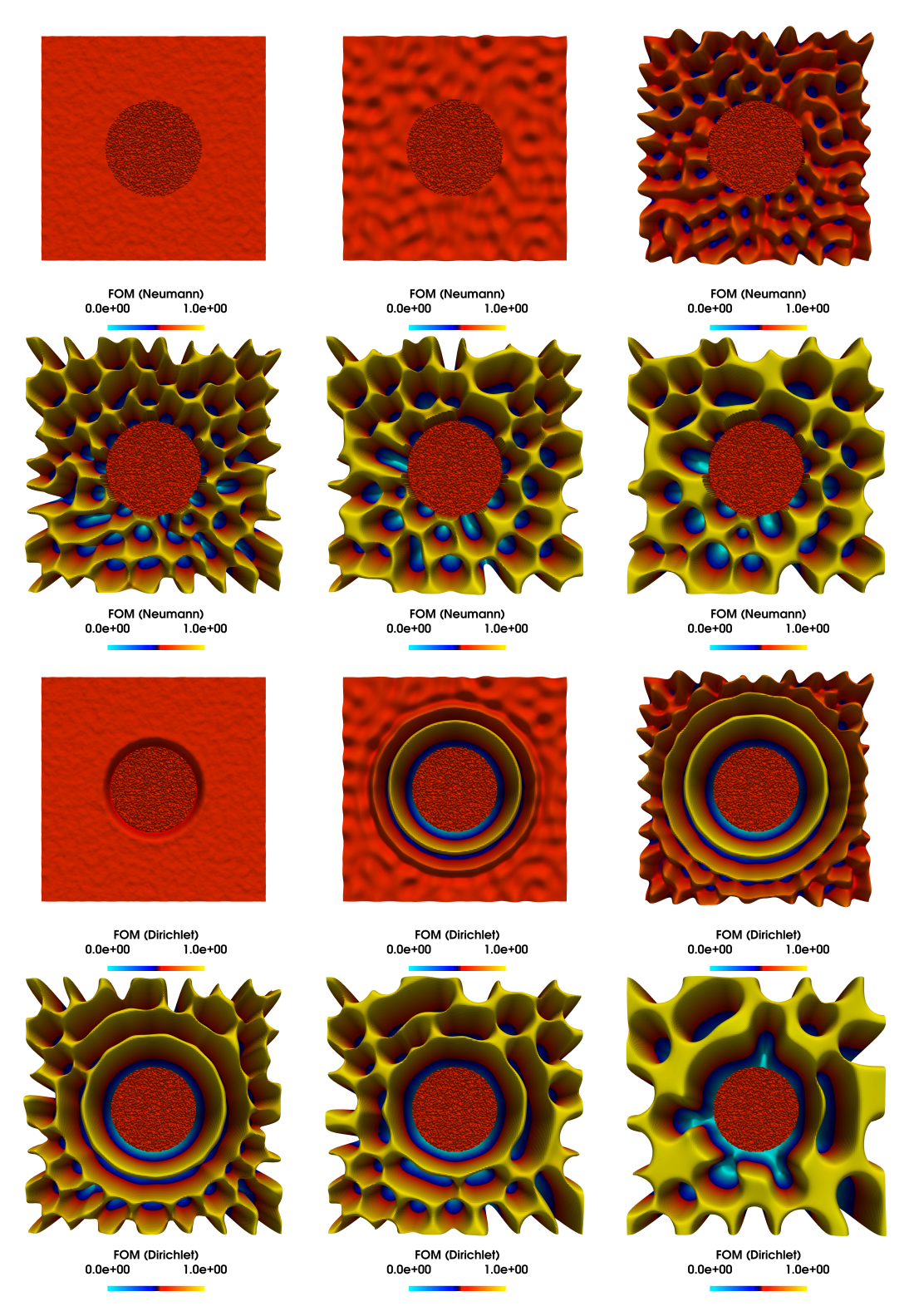


FIGURE 6. The full order solver and the concentration field (whole background geometry) for a fixed parameter  $\mu_{\text{test}} = 0.436$  at times  $t = [1, 25, 50, 120, 200, 500]\tau_n$  and mesh size h = 1/96.

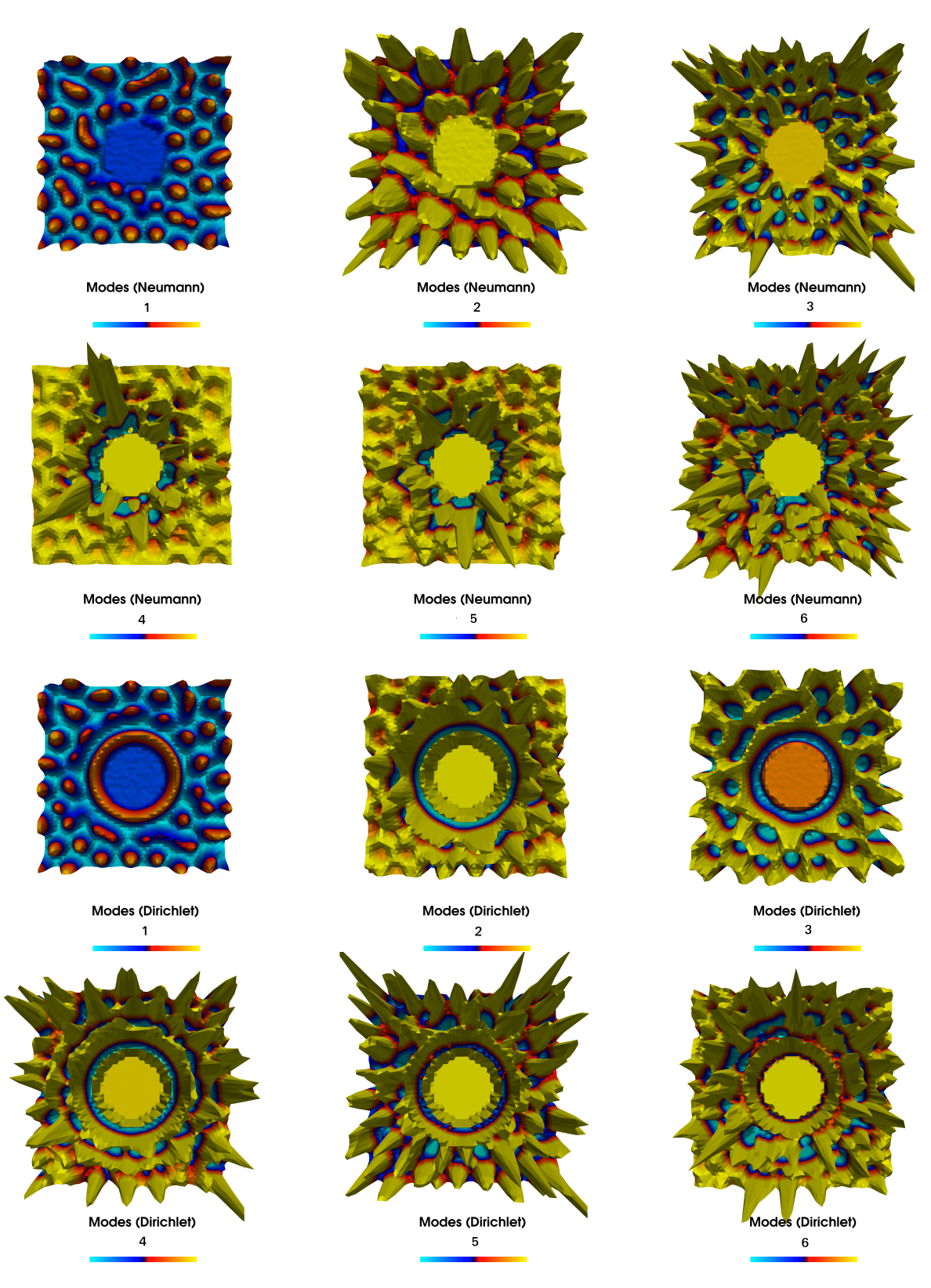


FIGURE 7. The first 6 basis components for concentration u considering Neumann and Dirichlet geometrical parametrization for  $\mu \in [0.36, 0.48]$ .

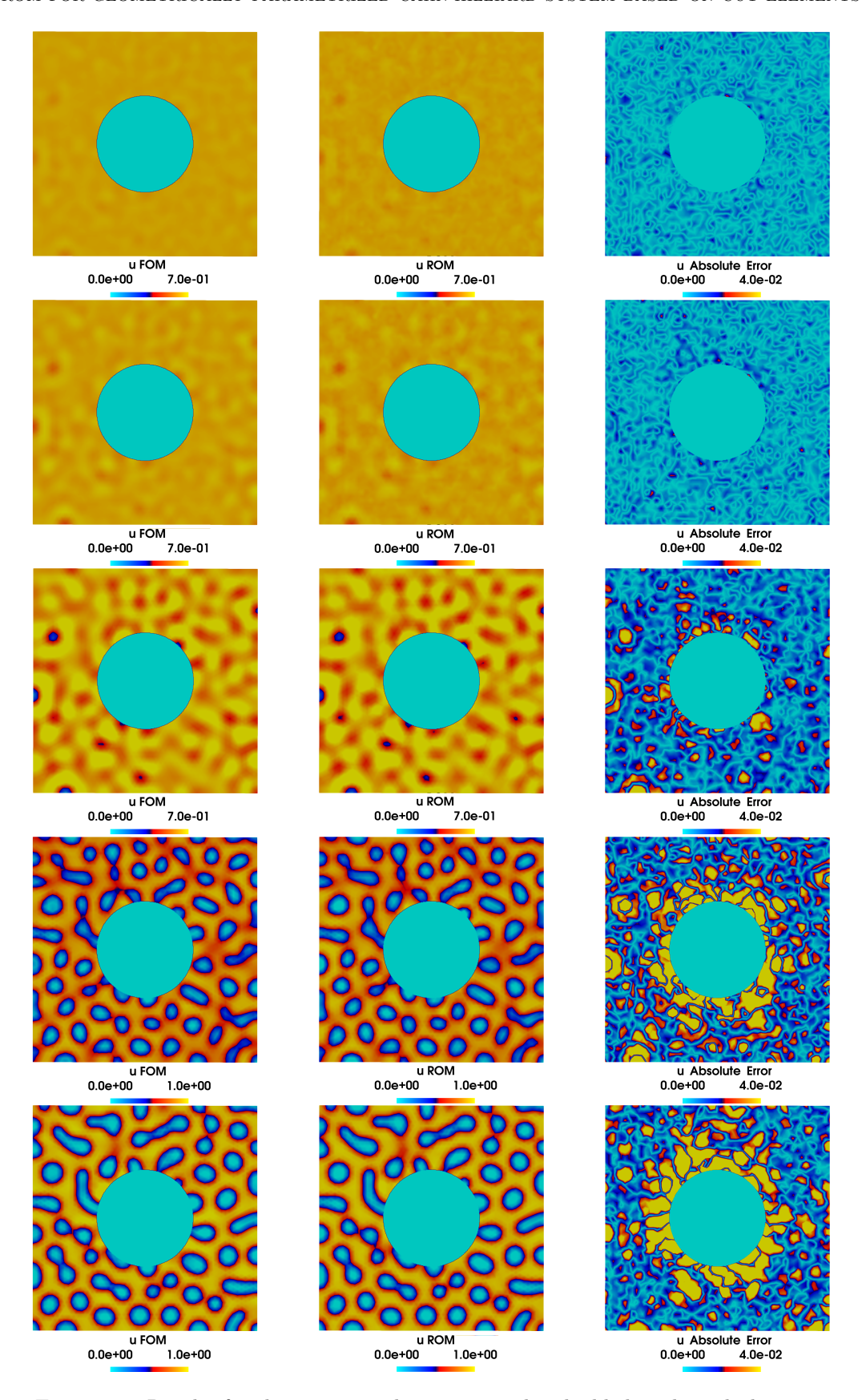


FIGURE 8. Results for the geometrical parametrized embedded circle with diameter  $\mu_{\text{test}} = 0.436$  and open boundary. In the first, second and third column we report the full-order solution, the reduced order solution and the absolute error plots for the concentration field. Each row corresponds to a different time  $t = [10, 20, 40, 60, 100]\tau_n$ .

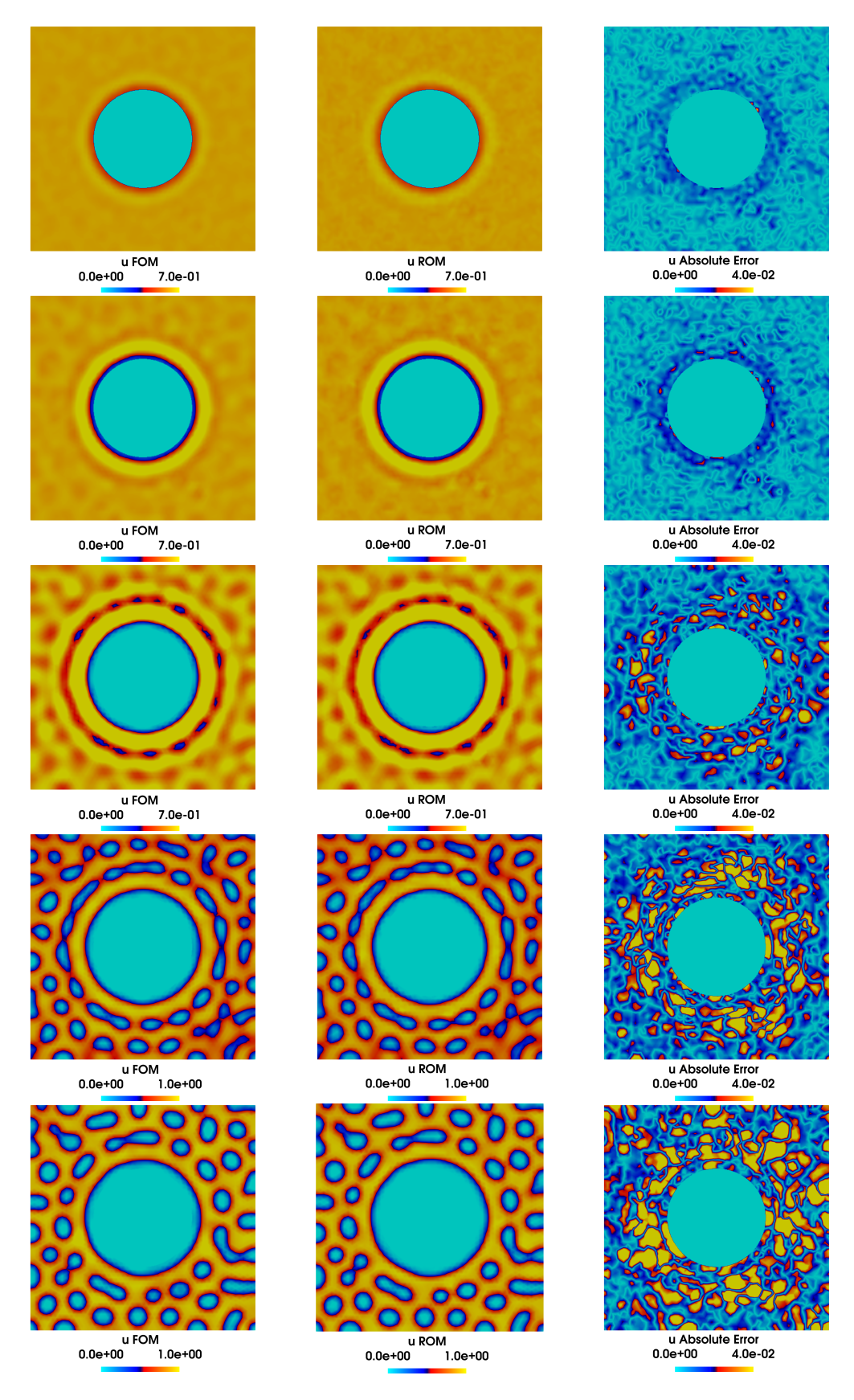


FIGURE 9. Results for the geometrical parametrized embedded circle with diameter  $\mu_{\text{test}} = 0.436$  and *Dirichlet embedded boundary*. In the first, second and third column we report the full-order solution, the reduced order solution and the absolute error plots for the concentration field. Each row corresponds to a different time  $t = [10, 20, 40, 60, 100]\tau_n$ .

Snapshots for:	900 train parameters				
Modes	Relative error for Neumann case		Relative error for Dirichlet case		
(N)	Concentration $u$	Potential w	Concentration $u$	Potential w	
1	0.18370	0.49895	0.22298	0.96624	
5	0.15292	0.41387	0.20528	0.37814	
10	0.06069	0.18397	0.11857	0.28665	
15	0.04086	0.11956	0.08977	0.21658	
20	0.04046	0.11311	0.07631	0.18301	
25	0.03498	0.09183	0.04808	0.13259	
30	0.02883	0.07852	0.03932	0.10802	
35	0.02641	0.07085	0.03284	0.09350	
40	0.02063	0.05981	0.02879	0.08377	
45	0.01987	0.05681	0.02749	0.08072	

Table 1. Geometrical parametrization and the relative error between the full-order solution and the reduced basis solution for the concentration and potential component. Results are reported for different dimensions of the reduced basis spaces.

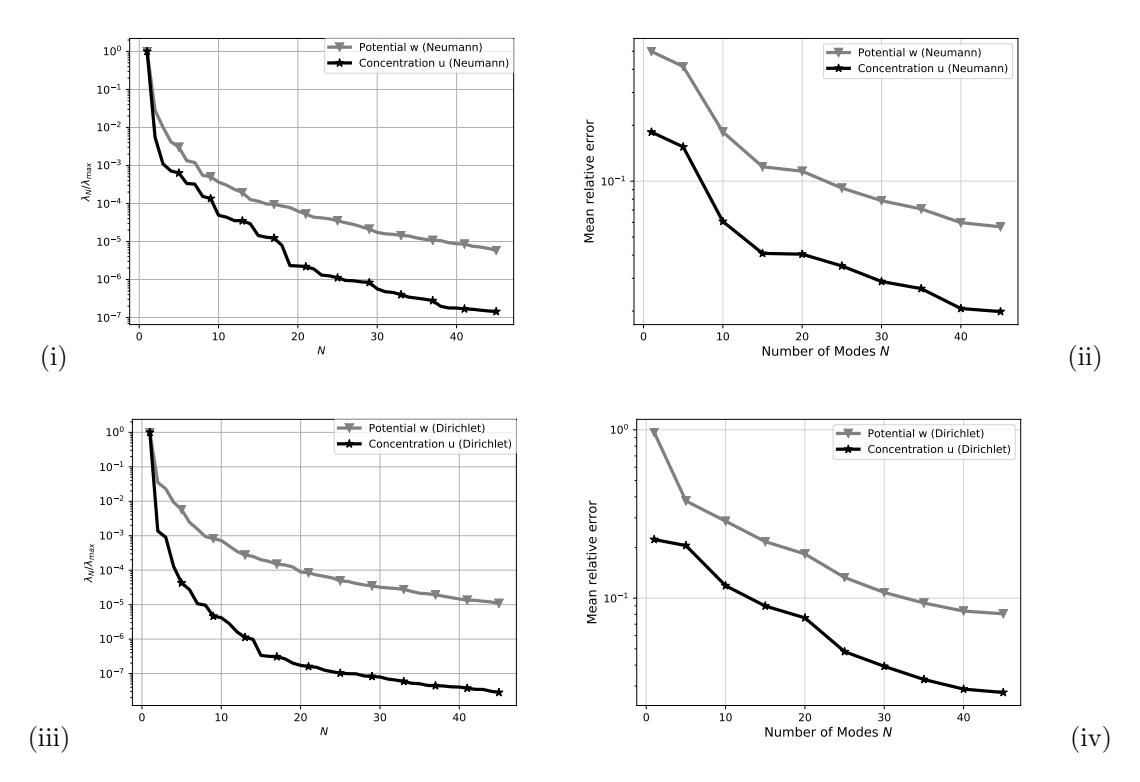


FIGURE 10. Geometrical parametrization and visualization of the results. The left plots depict the eigenvalues decay with respect to the numbers of the modes for the concentration and potential variable. On the right plots, we visualize the relative errors of the reduced-order problem for one random parameter value and for various number of modes.

As it is displayed in Figures 8 and 9 –Neumann and Dirichlet embedded boundary experiments respectively– and with a minds eye comparison of the FOM and ROM solutions in first and second column, with a brief look they seem identical for every row associated to the time instances  $t = [10, 20, 40, 60, 100]\tau_n$ . In the third column and looking from a more detailed point of view, the absolute error in each point of the geometry domain is visualized for the open boundary and the Dirichlet case. In Table 1 and again for both types of boundaries, the relative errors for the concentration phase field for various number of basis components are reported and their graph can be seen in Figure 10 as well as the eigenvalues and their decay which have been used for the ROM. Thereafter, for a better

Snapshots for:	900 train parameters			
Modes	execution times	Savings		
(N)	(t)	$(t_{\rm FOM} - t_{\rm RB})/t_{\rm FOM}$		
1	0.02808	99.718%		
10	0.05299	99.468%		
20	0.08422	99.154%		
30	0.10766	98,919%		
40	0.14128	98.581%		
45	0.16291	98.364%		

Table 2. Execution time at the reduced order level and per cent (%) savings. The computational time includes the projection of the full order matrices, the execution time of the online solver and the resolution of the reduced problem. Times are for the resolution of one random value of the input parameter. The time execution at full order method level (FOM) is equal to  $\approx 9.9623$  sec.

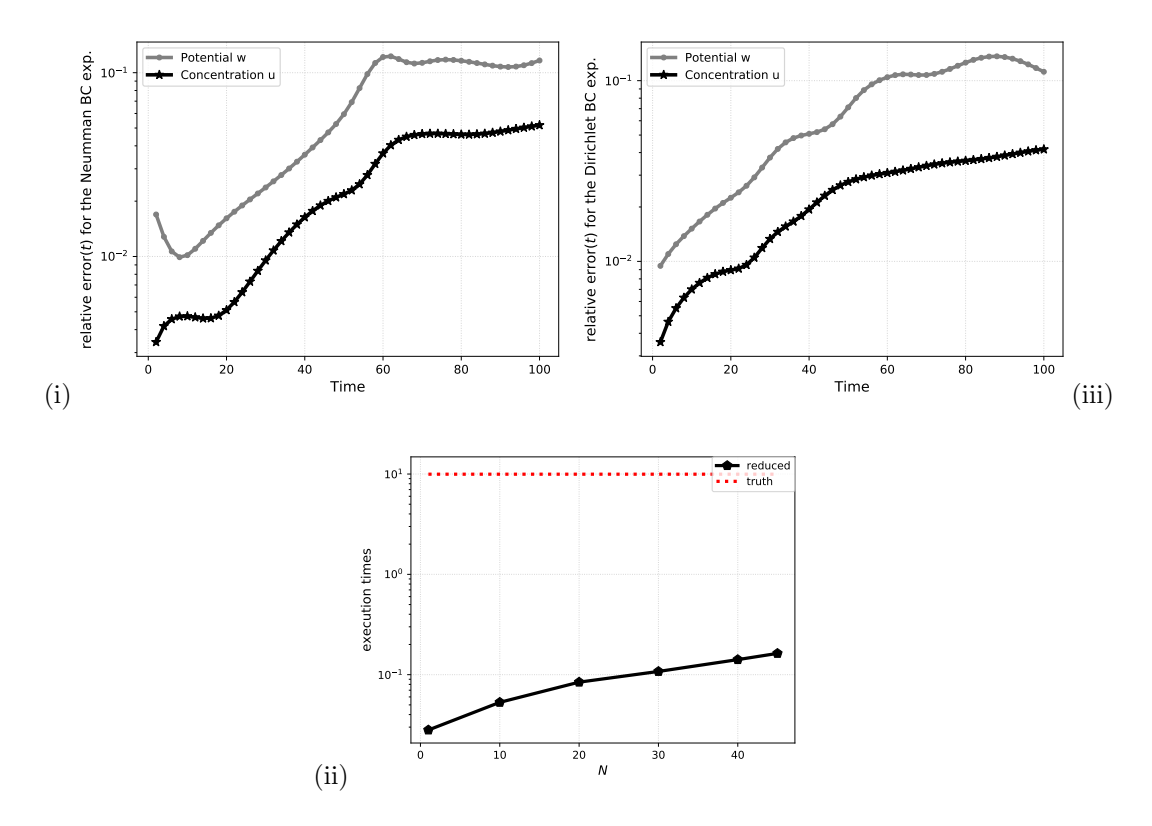


FIGURE 11. Time related results, and visualization for the Neumann and Dirichlet case. The left and right plots depict the relative errors with respect the time for the concentration and potential variable and 45 modes. On the bottom plot, we visualize the execution times of the reduced-order problem for one random parameter value and for various number of modes.

understanding, the relative errors evolution with respect to time, for a 45 modes test, is demonstrated in Table 3 and visualized in Figure 11 (i), (iii). Finally in Table 2, and in Figure 11 (ii) we report the execution times for various number of basis components including the projection of the full order matrices, the execution time of the online solver and the determination of the reduced problem and we compare them with the time execution at the full order level, namely 9.9623 sec.

4.2.1. Some comments. Numerical experiments consider open boundary conditions as well as Dirichlet ones. The tests clearly indicate that an efficient orthogonal decomposition projection-based reduced-order model can be derived over a full-order cut finite element method solver for the challenging (for both the full and the reduced level, see also the uncomfort basis components in Figure 7) nonlinear

Snapshots for:	900 train parameters				
time $(i \times \tau_n)$	Relative error (Neumann)		Relative error (Dirichlet)		
i	Concentration u	Potential w	Concentration u	Potential w	
1	0.00342	0.01692	0.00357	0.00944	
10	0.00472	0.01016	0.00699	0.01517	
20	0.00510	0.01613	0.00894	0.02250	
30	0.00952	0.02374	0.01330	0.03751	
40	0.01634	0.03580	0.01938	0.05078	
50	0.02184	0.05944	0.02752	0.07117	
60	0.03639	0.12172	0.03086	0.10452	
70	0.04636	0.11315	0.03381	0.10750	
80	0.04611	0.11615	0.03606	0.12585	
90	0.04787	0.10791	0.03856	0.13514	
100	0.05181	0.11652	0.04169	0.11201	

TABLE 3. The  $L^2$  relative error norm is reported overtime for the concentration and potential field for the Neumann and Dirichlet type of boundaries experiments. The ROMs have been obtained with 45 modes for the concentration for both cases.

Cahn–Hilliard system. Another aspect is that we avoid the costly traditional approach of geometric transformation in a reference domain and we rely only on an appropriate smooth enough background grid. Last Section tests have clearly shown that accurate results can be obtained for this phase-field system at a reduced level.

#### 5. Concluding remarks and future developments

We conclude this work by noting that the above approach and the combination of unfitted mesh finite element methods with an embedded POD basis and IMEX type discretization, by using linear polynomials, imply good reduced basis approximation properties for a Cahn-Hilliard fourth-order diffusion nonlinear PDE system. Considering the reduced-order approximation, the background mesh approach appears beneficial even for nonsmooth pseudo-random initial data. As expected, and referring to previous related authors' works, [55, 54], an increased error is noticed onto the Nitsche embedded boundary interface in the reduced level, which will be studied elsewhere. We underline the significant execution time reduction considering the projection of the full order matrices, through the reduced execution time of the online solver and the resolution of the reduced problem, by capturing efficiently the full order solution information in a reduced level solution. As a perspective, we mention the construction of higher-order IMEX methods, more efficient methodologies for the affine decomposition of the discretization differential operator, and the investigation of the applicability of well-known hyper reduction techniques, such as the empirical interpolation method, [40], in the context of the aforementioned embedded reduced-order basis method. Of future interest also parabolic nonlinear partial differential equations set in a more general framework and to test snapshots transportation techniques as presented in [52].

#### ACKNOWLEDGMENTS

This work is supported by the European Research Council Executive Agency by means of the H2020 ERC Consolidator Grant project AROMA-CFD "Advanced Reduced Order Methods with Applications in Computational Fluid Dynamics" - GA 681447, (PI: Prof. G. Rozza), FARE-X-AROMA-CFD project by MIUR, INdAM-GNCS 2018 and 2019 and by project FSE - European Social Fund - HEaD "Higher Education and Development" SISSA operazione 1, Regione Autonoma Friuli - Venezia Giulia, the Hellenic Foundation for Research and Innovation (HFRI) and the General Secretariat for Research and Technology (GSRT), under grant agreement No[1115] and National Infrastructures for Research and Technology S.A. (GRNET S.A.) in the National HPC facility - ARIS - under project ID pa190902. The authors would like also to thank Dr Andrea Mola for useful instructions regarding the cutfem stabilization, and Dr Francesco Ballarin for fruitful discussions for the reduced order part. Numerical simulations have been obtained with ngsxfem/ngsolve [85, 86, 84] and RBniCS [87]; we acknowledge developers and contributors of each of the aforementioned software packages.

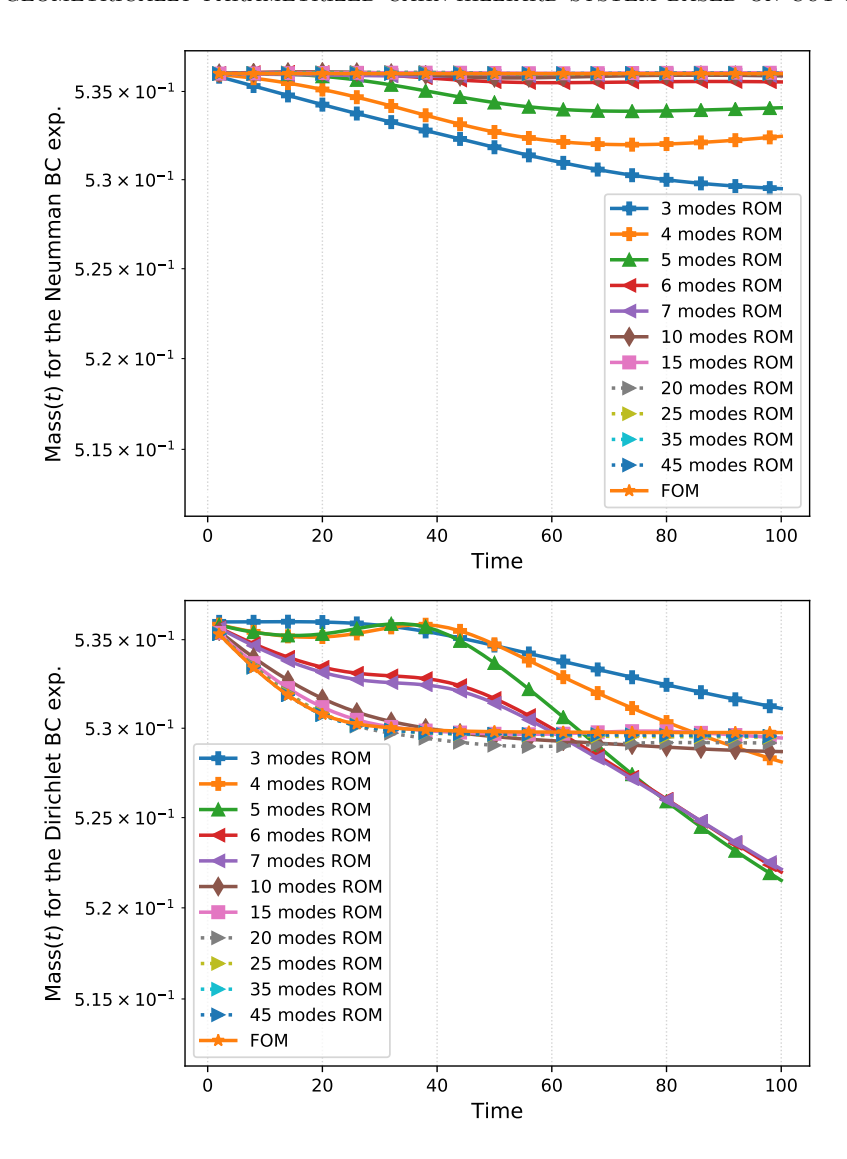


FIGURE 12. The conservation of mass for Neumann and Dirichlet embedded boundaries, evolutionary with respect to time, together with its RB approximation is reported and verified in FOM and ROM level for various number of modes as considered in the numerical examples, for the parameter value  $\mu = 0.436$  and time instances  $t = n\tau_n$ , for n = 1, ..., 100.

# References

- [1] Agosti, A., Antonietti, P.F., Ciarletta, P., Grasselli, M., Verani, M.: A Cahn-Hilliard-type equation with application to tumor growth dynamics. Mathematical Methods in the Applied Sciences 40(18), 7598–7626 (2017)
- [2] Alikakos, N., Fusco, G., Smyrnelis, P.: Elliptic Systems of Phase Transition Type. 91. Monograph in the series Progress in Nonlinear Differential Equations and Their Applications, Birkhauser (2018)
- [3] Alpak, F.O., Riviere, B., Frank, F.: A phase-field method for the direct simulation of two-phase flows in pore-scale media using a non-equilibrium wetting boundary condition. Computational Geosciences **20**(5), 881–908 (2016)
- [4] Anderson, D.M., McFadden, G.B., Wheeler, A.A.: Diffuse-interface methods in fluid mechanics. Annual Review of Fluid Mechanics 30(1), 139–165 (1998)
- [5] Antonopoulou, D.C., Karali, G., Millet, A.: Existence and regularity of solution for a stochastic Cahn–Hilliard/Allen-Cahn equation with unbounded noise diffusion (2013)
- [6] Antonopoulou, D.C., Karali, G., Millet, A.: Existence and regularity of solution for a stochastic Cahn—Hilliard/Allen-Cahn equation with unbounded noise diffusion. Journal of Differential Equations 260(3), 2383 2417 (2016)
- [7] Balajewicz, M., Farhat, C.: Reduction of nonlinear embedded boundary models for problems with evolving interfaces. Journal of Computational Physics 274, 489–504 (2014)

- [8] Ballarin, F., Manzoni, A., Quarteroni, A., Rozza, G.: Supremizer stabilization of POD-Galerkin approximation of parametrized steady incompressible Navier–Stokes equations. International Journal for Numerical Methods in Engineering 102(5), 1136–1161 (2015)
- [9] Benner, P., Ohlberger, M., Patera, A., Rozza, G., Urban, K.: Model Reduction of Parametrized Systems, MS&A series, vol. 17. Springer (2017)
- [10] Bertozzi, A.L., Esedoglu, S., Gillette, A.: Inpainting of Binary Images Using the Cahn–Hilliard Equation. Trans. Img. Proc. 16(1), 285–291 (2007)
- [11] Blank, L., Garcke, H., Sarbu, L., Srisupattarawanit, T., Styles, V., Voigt, A.: Phase-field Approaches to Structural Topology Optimization, pp. 245–256. Springer Basel, Basel (2012)
- [12] Bosch, J.: Fast Iterative Solvers for Cahn-Hilliard Problems. Ph.D. thesis, Otto-von-Guericke Universitat, Magdeburg (2016)
- [13] Burman, E.: Ghost penalty. Comptes Rendus Mathematique 348(21), 1217 1220 (2010)
- [14] Burman, E., Hansbo, P.: Fictitious domain finite element methods using cut elements: II. A stabilized Nitsche method. Applied Numerical Mathematics 52(6), 2837–2862 (2011)
- [15] Burman, E., Hansbo, P.: Fictitious domain methods using cut elements: III. A stabilized Nitsche method for Stokes' problem. ESAIM: M2AN 48(5-8), 859–874 (2014)
- [16] Cahn, J.W., Hilliard, J.E.: Free Energy of a Nonuniform System. I. Interfacial Free Energy. The Journal of Chemical Physics 28(2), 258–267 (1958)
- [17] Chave, F., Di Pietro, D., Marche, F., Pigeonneau, F.: A Hybrid High-Order Method for the Cahn-Hilliard problem in Mixed Form. SIAM Journal on Numerical Analysis 54(3), 1873–1898 (2016)
- [18] Cherfils, L., Fakih, H., Miranville, A.: A Complex Version of the Cahn-Hilliard Equation for Grayscale Image Inpainting. Multiscale Modeling & Simulation 15(1), 575-605 (2017)
- [19] Chinesta, F., Huerta, A., Rozza, G., Willcox, K.: chap. Model Reduction Methods, Encyclopedia of Computational Mechanics, Second Edition, pp. 1–36. John Wiley & Sons (2017)
- [20] Chinesta, F., Ladeveze, P., Cueto, E.: A Short Review on Model Order Reduction Based on Proper Generalized Decomposition. Archives of Computational Methods in Engineering 18(4), 395 (2011)
- [21] Choksi, R., Peletier, M., Williams, J.: On the Phase Diagram for Microphase Separation of Diblock Copolymers: An Approach via a Nonlocal Cahn–Hilliard Functional. SIAM Journal on Applied Mathematics **69**(6), 1712–1738 (2009)
- [22] Chrysafinos, K., Karatzas, E.N.: Error Estimates for Discontinuous Galerkin Time-Stepping Schemes for Robin Boundary Control Problems Constrained to Parabolic PDEs. SIAM Journal on Numerical Analysis 52(6), 2837–2862 (2014)
- [23] Chrysafinos, K., Karatzas, E.N.: Symmetric error estimates for discontinuous Galerkin time-stepping schemes for optimal control problems constrained to evolutionary Stokes equations. Computational Optimization and Applications 60(3), 719–751 (2015)
- [24] Claus, S., Kerfriden, P.: A cutfem method for two-phase flow problems. Computer Methods in Applied Mechanics and Engineering 348, 185 206 (2019)
- [25] Colli, P., Farshbaf-Shaker, M., Gilardi, G., Sprekels, J.: Optimal Boundary Control of a Viscous Cahn-Hilliard System with Dynamic Boundary Condition and Double Obstacle Potentials. SIAM Journal on Control and Optimization 53(4), 2696–2721 (2015)
- [26] De Groot, S., Mazur, P.: Non-equilibrium thermodynamics. (1962), Dover edition (2013)
- [27] Dumon, A., Allery, C., Ammar, A.: Proper general decomposition (PGD) for the resolution of Navier–Stokes equations. Journal of Computational Physics 230(4), 1387–1407 (2011)
- [28] Elliott, C., Larsson, S.: Error estimates with smooth and nonsmooth data for a finite element method for the Cahn-Hilliard equation. Math. Comp. **58**(S33-S36), 603-630 (1992)
- [29] Elliott, C.M.: The Cahn-Hilliard Model for the Kinetics of Phase Separation, pp. 35–73. Birkhäuser Basel, Basel (1989)
- [30] Elliott, C.M., French, D.A., Milner, F.A.: A second order splitting method for the Cahn-Hilliard equation. Numerische Mathematik 54(5), 575–590 (1989)
- [31] Elliott, C.M., Songmu, Z.: On the Cahn-Hilliard equation. Archive for Rational Mechanics and Analysis 96(4), 339–357 (1986)
- [32] Embar, A., Dolbow, J., Harari, I.: Imposing dirichlet boundary conditions with Nitsche's method and spline-based finite elements. International Journal for Numerical Methods in Engineering 83(7), 877–898 (2010)
- [33] Furihata, D., Kovàcs, M., Larsson, S., Lindgren, F.: Strong Convergence of a Fully Discrete Finite Element Approximation of the Stochastic Cahn-Hilliard Equation. SIAM Journal on Numerical Analysis 56(2), 708-731 (2018)
- [34] Goudenège, L., Martin, D., Vial, G.: High Order Finite Element Calculations for the Cahn-Hilliard Equation. Journal of Scientific Computing **52**(2), 294–321 (2012)
- [35] Gräßle, C., Hinze, M., Scharmacher, N.: POD for Optimal Control of the Cahn-Hilliard System Using Spatially Adapted Snapshots. In: F.A. Radu, K. Kumar, I. Berre, J.M. Nordbotten, I.S. Pop (eds.) Numerical Mathematics and Advanced Applications ENUMATH 2017, pp. 703–711. Springer International Publishing (2019)
- [36] Grepl, M., Maday, Y., Nguyen, N., Patera, A.: Efficient reduced-basis treatment of nonaffine and nonlinear partial differential equations. ESAIM: M2AN 41(3), 575–605 (2007)
- [37] Grepl, M., Patera, A.: A posteriori error bounds for reduced-basis approximations of parametrized parabolic partial differential equations. ESAIM: M2AN 39(1), 157–181 (2005)
- [38] Gurtin, M.E., Polignone, D., Vinals, J.: Two-phase binary fluids and immiscible fluids described by an order parameter. Mathematical Models and Methods in Applied Sciences 06(06), 815–831 (1996)
- [39] Haasdonk, B., Ohlberger, M.: Reduced basis method for finite volume approximations of parametrized linear evolution equations. Mathematical Modelling and Numerical Analysis 42(2), 277–302 (2008)

- [40] Haasdonk, B., Ohlberger, M., Rozza, G.: A reduced basis method for evolution schemes with parameter-dependent explicit operators. Electron. Trans. Numer. Anal. 32, 145–161 (2008)
- [41] Harari, I., Grosu, E.: A unified approach for embedded boundary conditions for fourth-order elliptic problems. International Journal for Numerical Methods in Engineering 104(7), 655–675 (2015)
- [42] Hesthaven, J., Rozza, G., Stamm, B.: Certified Reduced Basis Methods for Parametrized Partial Differential Equations. SpringerBriefs in Mathematics. Springer International Publishing (2016)
- [43] Hintermüller, M., Hinze, M., Kahle, C.: An Adaptive Finite Element Moreau-Yosida-based Solver for a Coupled Cahn-Hilliard/Navier-Stokes System. J. Comput. Phys. **235**(C), 810–827 (2013)
- [44] Hintermüller, M., Keil, T., Wegner, D.: Optimal Control of a Semidiscrete Cahn-Hilliard-Navier-Stokes System with Nonmatched Fluid Densities. SIAM Journal on Control and Optimization **55**(3), 1954–1989 (2017)
- [45] Hintermuller, M., Wegner, D.: Distributed Optimal Control of the Cahn-Hilliard System Including the Case of a Double-Obstacle Homogeneous Free Energy Density. SIAM Journal on Control and Optimization **50**(1), 388–418 (2012)
- [46] Hinze, M., Kahle, C.: A Nonlinear Model Predictive Concept for Control of Two-Phase Flows Governed by the Cahn-Hilliard Navier-Stokes System. In: D. Hömberg, F. Tröltzsch (eds.) System Modeling and Optimization, pp. 348–357. Springer Berlin Heidelberg, Berlin, Heidelberg (2013)
- [47] Israelachvili, J.N.: Intermolecular and Surface Forces. Elsevier (2011)
- [48] Jeong, D., Kim, J.: Microphase separation patterns in diblock copolymers on curved surfaces using a nonlocal Cahn-Hilliard equation. The European Physical Journal E 38(11), 117 (2015)
- [49] Junseok, K., Seunggyu, L., Yongho, C., Seok-Min, L., Darae, J.: Basic Principles and Practical Applications of the Cahn-Hilliard Equation. Mathematical Problems in Engineering (1), 79–141 (2016)
- [50] Kalashnikova, I., Barone, M.F.: On the stability and convergence of a Galerkin reduced order model (ROM) of compressible flow with solid wall and far-field boundary treatment. International Journal for Numerical Methods in Engineering 83(10), 1345–1375 (2010)
- [51] Karali, G., Nagase, Y.: On the existence of solution for a Cahn-Hilliard/Allen-Cahn equation. Discrete and Continuous Dynamical Systems S 7(1937-1632\_2014\_1\_127), 127 (2014)
- [52] Karatzas, E.N., Ballarin, F., Rozza, G.: Projection-based reduced order models for a cut finite element method in parametrized domains. Computers & Mathematics with Applications **79**(3), 833 851 (2020)
- [53] Karatzas, E.N., Nonino, M., Ballarin, F., Rozza, G.: A Reduced order cut finite element basis for stationary and evolutionary geometrically parameterized Navier–Stokes systems (2020). In preparation.
- [54] Karatzas, E.N., Stabile, G., Atallah, N., Scovazzi, G., Rozza, G.: A Reduced Order Approach for the Embedded Shifted Boundary FEM and a Heat Exchange System on Parametrized Geometries In: Fehr J., Haasdonk B. (eds) IUTAM Symposium on Model Order Reduction of Coupled Systems, Stuttgart, Germany, May 22–25, 2018. IUTAM Bookseries, vol 36. Springer, Cham (2020)
- [55] Karatzas, E.N., Stabile, G., Nouveau, L., Scovazzi, G., Rozza, G.: A reduced basis approach for PDEs on parametrized geometries based on the shifted boundary finite element method and application to a Stokes flow. Computer Methods in Applied Mechanics and Engineering 347, 568 587 (2019)
- [56] Karatzas, E.N., Stabile, G., Nouveau, L., Scovazzi, G., Rozza, G.: A reduced-order shifted boundary method for parametrized incompressible Navier-Stokes equations. Computer Methods in Applied Mechanics and Engineering 370, 113-273 (2020)
- [57] Katsouleas, G., Karatzas, E.N., Travlopanos, F.: Cut finite element error estimates for a class of nonlinear elliptic PDEs. pp. 1–6. Loughborough University, doi: 10.17028/rd.lboro.12154854.v1, extended version at arXiv:2003.06489 (2020)
- [58] Kunisch, K., Volkwein, S.: Galerkin proper orthogonal decomposition methods for a general equation in fluid dynamics. SIAM Journal on Numerical Analysis **40**(2), 492–515 (2002)
- [59] Lehrenfeld, C., Reusken, A.: L2-error analysis of an isoparametric unfitted finite element method for elliptic interface problems. pp. 85–99. Journal of Numerical Mathematics (2019)
- [60] Li, C., Qin, R., Ming, J., Wang, Z.: A discontinuous Galerkin method for stochastic Cahn–Hilliard equations. Computers & Mathematics with Applications **75**(6), 2100 2114 (2018). 2nd Annual Meeting of SIAM Central States Section, September 30-October 2, 2016
- [61] Li, Y., Jeong, D., Shin, J., Kim, J.: A conservative numerical method for the Cahn–Hilliard equation with Dirichlet boundary conditions in complex domains. Computers & Mathematics with Applications 65(1), 102 115 (2013)
- [62] Novick-Cohen, A., Segel, L.A.: Nonlinear aspects of the Cahn-Hilliard equation. Physica D: Nonlinear Phenomena 10(3), 277 – 298 (1984)
- [63] Quarteroni, A., Manzoni, A., Negri, F.: Reduced Basis Methods for Partial Differential Equations, vol. 92. UNI-TEXT/La Matematica per il 3+2 book series, Springer International Publishing (2016)
- [64] Regazzoni, F., Parolini, N., Verani, M.: Topology optimization of multiple anisotropic materials, with application to self-assembling diblock copolymers. Computer Methods in Applied Mechanics and Engineering 338, 562 596 (2018)
- [65] Reshma, S., Hansa J Thattil, H.: Inpainting of Binary Images Using the Cahn-Hilliard Equation. International Journal of Computer Science Engineering and Technology 4(11), 296–300 (2014)
- [66] Rocca, E., Sprekels, J.: Optimal Distributed Control of a Nonlocal Convective Cahn–Hilliard Equation by the Velocity in Three Dimensions. SIAM Journal on Control and Optimization **53**(3), 1654–1680 (2015)
- [67] Rokhzadi, A.: IMEX and Semi-Implicit Runge-Kutta Schemes for CFD Simulations. Ph.D. thesis, Civil Engineering Department, Faculty of Engineering, University of Ottawa (2018)
- [68] Rozza, G.: Reduced Basis Methods for Elliptic Equations in subdomains with A-Posteriori Error Bounds and Adaptivity. App. Num. Math. 55(4), 403–424 (2005)
- [69] Rozza, G.: Reduced basis methods for Stokes equations in domains with non-affine parameter dependence. Computing and Visualization in Science 12(1), 23–35 (2009)

- [70] Rozza, G., Huynh, D., Patera, A.: Reduced basis approximation and a posteriori error estimation for affinely parametrized elliptic coercive partial differential equations: Application to transport and continuum mechanics. Archives of Computational Methods in Engineering 15(3), 229–275 (2008)
- [71] Rozza, G., Huynh, D.B.P., Manzoni, A.: Reduced basis approximation and a posteriori error estimation for Stokes flows in parametrized geometries: Roles of the inf-sup stability constants. Numerische Mathematik 125(1), 115–152
- [72] Rozza, G., Veroy, K.: On the stability of the reduced basis method for Stokes equations in parametrized domains. Computer Methods in Applied Mechanics and Engineering 196(7), 1244–1260 (2007)
- Schott, B.: Stabilized Cut Finite Element Methods for Complex Interface Coupled Flow Problems. Ph.D. thesis, Technische Universität München (TUM) (2016)
- [74] Shenyang, H.: Phase-field Models of Microstructure Evolution in a System with Elastic Inhomogeneity and Defects. Ph.D. thesis, Pennsylvania State University, Department of Materials Science and Engineering (2004)
- [75] Veroy, K., Prud'homme, C., Patera, A.: Reduced-basis approximation of the viscous Burgers equation: rigorous a posteriori error bounds. Comptes Rendus Mathematique 337(9), 619-624 (2003)
- Wells, G.N., Kuhl, E., Garikipati, K.: A discontinuous Galerkin method for the Cahn-Hilliard equation. Journal of Computational Physics **218**(2), 860 – 877 (2006)
- [77] Welper, G.: Optimal treatment for a phase field system of Cahn-Hilliard type modeling tumor growth by asymptotic scheme (2019). ArXiv:1902.01079v2
- [78] Wodo, O., Ganapathysubramanian, B.: Computationally efficient solution to the Cahn-Hilliard equation: Adaptive implicit time schemes, mesh sensitivity analysis and the 3D isoperimetric problem. Journal of Computational Physics **230**(15), 6037 – 6060 (2011)
- [79] Xu, M., Guo, H., Zou, Q.: Hessian recovery based finite element methods for the Cahn-Hilliard equation. Journal of Computational Physics 386, 524 - 540 (2019)
- [80] Zhang, X., Li, H., Liu, C.: Optimal Control Problem for the Cahn-Hilliard/Allen-Cahn Equation with State Constraint. Applied Mathematics & Optimization (2018)
- [81] Zhao, X., Liu, C.: Optimal Control for the Convective Cahn-Hilliard Equation in 2D Case. Applied Mathematics & Optimization **70**(1), 61-82 (2014)
- [82] Zhao, Y., Schillinger, D., Xu, B.X.: Variational boundary conditions based on the Nitsche method for fitted and unfitted isogeometric discretizations of the mechanically coupled Cahn-Hilliard equation. Journal of Computational Physics **340**, 177 – 199 (2017)
- [83] Zhou, S., Wang, M.Y.: Multimaterial structural topology optimization with a generalized Cahn-Hilliard model of multiphase transition. Structural and Multidisciplinary Optimization 33(2), 89 (2006)
- [84] Schöberl, J.: C++11 implementation of finite elements in NGSolve. Institute for Analysis and Scientific Computing, Vienna University of Technology (2014)
- [85] ngsxfem Add-On to NGSolve for unfitted finite element discretizations. https://github.com/ngsxfem/ngsxfem
- [86] NGSolve high performance multiphysics finite element software. https://github.com/NGSolve/ngsolve (2018)
- [87] RBniCS reduced order modelling in FEniCS. https://www.rbnicsproject.org (2015)